Cartesian Methods for the Shallow Water Equations on a Sphere

Paul Swarztrauber, Dave Williamson, John B. Drake

June 5, 1996

Abstract

A Cartesian method is used in conjunction with the shallow water equations and a spatial discretization based on the Cartesian form of the spherical harmonics. Updates of the momentum equation are accomplished using collocation with spherical harmonics. Computational velocities are expressed in Cartesian coordinates so that no problem with a singularity at the pole is encountered. The geopotential (height) equation is discretized in a similar fashion with a collocation of the divergence term. Error measures and conservation properties of the method are reported for a standard set of test problems.

1 Introduction

This report is one of a series of documents concerning the use of numerical methods for global climate modeling. The work reported is sponsored by the CHAMMP initiative of the Department of Energy's Office of Energy Research. CHAMMP is an acronym for Computer Hardware, Advanced Mathematics and Model Physics. Its goal is the development of advanced climate models with considerably improved throughput, accuracy and realism.

The use of triangular meshes for the solution of PDE's on a spherical domain is attractive for a number of reasons. First of all, triangles allow nearly uniform meshes. Rectangular meshes suffer the problem of varying resolution near the poles for the standard spherical coordinate projection. Secondly, triangles require only a simple data structure for use with adaptive mesh techniques or for meshes that resolve irregular features. Adapting a mesh to fit a coastline is an obvious example.

Williamson and several others investigated the use of icosahedral- triangular meshes in a series of early papers [9, 12, 13, 14, 15, 17]. The shallow water equations on the sphere served as a primary equation set for testing the numerical methods because of their relevance in atmospheric flow models. The review article by Williamson [16] gives further references.

More recently an icosahedral method based on the stream function and velocity potential formulation with a control volume discretization has been proposed by Masuda [6]. The method was tested on a standard set of cases [18] by Heikes and Randall in [3, 4]. Other icosahedral methods have been proposed in [2].

Our renewed interest in these methods springs from advances in computing and numerical analysis. The introduction of massively parallel computers has prompted the reexamination of many classical algorithms. The granularity of tasks that can be performed in parallel appears to be finer for the finite difference and finite element methods than for the prevailing spectral transform methods. This offers the possibility of effective use of many small processors of a parallel computer.

One of the problems encountered with the earlier triangular mesh formulations arose from the treatment of the advection terms in the shallow water equations. Recent advances in the numerical solution of hyperbolic equations and the development of higher order accurate shock capturing schemes also suggest that these methods need to be revisited.

The Cartesian form of the shallow water equations was proposed by Swarztrauber in [18]. It is an alternative formulation which avoids the singularity in the velocity at the pole by expressing velocities in a 3-D Cartesian form instead of in spherical coordinates. The formulation was used in conjunction with calculation of derivatives using a spectral vector harmonic method in [?]. In this paper we consider the Cartesian formulation in conjunction with the calculation of derivatives using a stencil of points located on an icosahedral grid.

2 The Shallow Water Equations on a Sphere

The momentum and mass continuity equations can be written in advective form

$$\frac{d\mathbf{v}}{dt} = -f\mathbf{k} \times \mathbf{v} - g\nabla h + \mathbf{F_v}, \tag{1}$$

and

$$\frac{dh^*}{dt} = -h^* \nabla \cdot \mathbf{v} + F_h \tag{2}$$

where the substantial derivative is given by

$$\frac{d}{dt}(\ ) \equiv \frac{\partial}{\partial t}(\ ) + \mathbf{v} \cdot \nabla(\ ). \tag{3}$$

The velocity is referred to a rotating Cartesian frame and the components of $\mathbf{v} = (u, v)$, are in the longitudinal and latitudinal directions respectively. The height is defined $h = h^* + h_s$. The bottom surface height is given by the time invariant function h_s. The external forcing, if present, is included in $\mathbf{F_v} = (F_u, F_v)$ and F_h.

This form of the equation is not in conservative form and consequently the numerical methods we develop will not be strictly conservative.

It may be advantageous to evaluate the surface derivatives using a Cartesian form. By extending the surface vector $\mathbf{v} = (u, v)^T$ to the three-dimensional $\mathbf{v}_s = (w, v, u)^T$ the shallow water equations can be embedded in the system

$$\frac{\partial \mathbf{v}_s}{\partial t} + \mathbf{S}(\mathbf{v}_s)\mathbf{v}_s + \boldsymbol{\alpha} + \boldsymbol{\beta} + \boldsymbol{\gamma} + \boldsymbol{\delta} = 0, \tag{4}$$

where

$$\mathbf{S}(\mathbf{v}_s) = \begin{pmatrix} \frac{\partial w}{\partial r} & \frac{1}{a}(\frac{\partial w}{\partial \theta} - v) & \frac{1}{a\cos\theta}(\frac{\partial w}{\partial \lambda} - u\cos\theta) \\ \frac{\partial v}{\partial r} & \frac{1}{a}(\frac{\partial v}{\partial \theta} + w) & \frac{1}{a\cos\theta}(\frac{\partial v}{\partial \lambda} - u\sin\theta) \\ \frac{\partial u}{\partial r} & \frac{1}{a}\frac{\partial u}{\partial \theta} & \frac{1}{a\cos\theta}(\frac{\partial u}{\partial \lambda} - v\sin\theta + w\cos\theta) \end{pmatrix}, \tag{5}$$

r is the radial coordinate ($r = a$ at the earth's surface) and

$$\boldsymbol{\alpha} = \begin{pmatrix} \frac{u^2+v^2}{a} \\ 0 \\ 0 \end{pmatrix}, \tag{6}$$

$$\boldsymbol{\beta} = \begin{pmatrix} 0 \\ \frac{g}{a}\frac{\partial h}{\partial \theta} \\ \frac{g}{a\cos\theta}\frac{\partial h}{\partial \lambda} \end{pmatrix}, \tag{7}$$

$$\boldsymbol{\gamma} = \begin{pmatrix} 0 \\ -F_v \\ -F_u \end{pmatrix}, \tag{8}$$

and

$$\boldsymbol{\delta} = \begin{pmatrix} 0 \\ fu \\ -fv \end{pmatrix}. \tag{9}$$

and If we define $\mathbf{V} = (X, Y, Z)^T$ as the velocity in Cartesian coordinates (x, y, z) then

$$\mathbf{v}_s = \mathbf{Q}\mathbf{V} \tag{10}$$

where

$$\mathbf{Q} = \begin{pmatrix} \cos\theta\cos\lambda & \cos\theta\sin\lambda & \sin\theta \\ -\sin\theta\cos\lambda & -\sin\theta\sin\lambda & \cos\theta \\ -\sin\lambda & \cos\lambda & 0 \end{pmatrix}. \tag{11}$$

Substituting (62) into (57) and multiplying by $\mathbf{Q}^T$ we obtain the Cartesian form

$$\frac{\partial \mathbf{V}}{\partial t} + \mathbf{C}\mathbf{V} + \mathbf{Q}^T(\boldsymbol{\alpha} + \boldsymbol{\beta} + \boldsymbol{\gamma} + \boldsymbol{\delta}) = 0. \tag{12}$$

In this equation

$$\mathbf{C} = \mathbf{Q}^T\mathbf{S}\mathbf{Q} = \begin{pmatrix} \frac{\partial X}{\partial x} & \frac{\partial X}{\partial y} & \frac{\partial X}{\partial z} \\ \frac{\partial Y}{\partial x} & \frac{\partial Y}{\partial y} & \frac{\partial Y}{\partial z} \\ \frac{\partial Z}{\partial x} & \frac{\partial Z}{\partial y} & \frac{\partial Z}{\partial z} \end{pmatrix}, \tag{13}$$

$$\mathbf{Q}^T\boldsymbol{\alpha} = \frac{1}{a^2}\begin{pmatrix} x(X^2+Y^2+Z^2) \\ y(X^2+Y^2+Z^2) \\ z(X^2+Y^2+Z^2) \end{pmatrix}, \tag{14}$$

$$\mathbf{Q}^T\boldsymbol{\delta} = \frac{2\Omega z}{a^2}\begin{pmatrix} 0 & -z & y \\ z & 0 & -x \\ -y & x & 0 \end{pmatrix}\begin{pmatrix} X \\ Y \\ Z \end{pmatrix}, \tag{15}$$

and

$$\mathbf{Q}^T\boldsymbol{\beta} = g\mathbf{P}\nabla_c h \tag{16}$$

where

$$\mathbf{P} = \frac{1}{a^2}\begin{pmatrix} a^2-x^2 & -xy & -xz \\ -xy & a^2-y^2 & -yz \\ -xz & -yz & a^2-z^2 \end{pmatrix}, \tag{17}$$

and

$$\nabla_c h = \left(\frac{\partial h}{\partial x}, \frac{\partial h}{\partial y}, \frac{\partial h}{\partial z}\right)^T. \tag{18}$$

Similarly the continuity equation in Cartesian form is

$$\frac{\partial h^*}{\partial t} + \mathbf{V}^T\mathbf{P}\nabla_c h^* + h^*\nabla_c\cdot\mathbf{V} = F_h. \tag{19}$$

The matrix P projects an arbitrary Cartesian vector onto a plane that is tangent to the sphere at the point (x, y, z).

2.1 Rotational Form of the Momentum Equation

Using the vector identity

$$\mathbf{v}\cdot\nabla\mathbf{v} = \nabla(\frac{\mathbf{v}\cdot\mathbf{v}}{2}) + \zeta\mathbf{k}\times\mathbf{v}, \tag{20}$$

the momentum equation can be written

$$\frac{\partial\mathbf{v}}{\partial t} = -(\zeta+f)\mathbf{k}\times\mathbf{v} - \nabla(gh + \frac{\mathbf{v}\cdot\mathbf{v}}{2}) + \mathbf{F}_{\mathbf{v}}. \tag{21}$$

Changing variables to Cartesian velocities the resulting Cartesian equation is

$$\frac{\partial\mathbf{V}}{\partial t} + \mathbf{Q}^T(\boldsymbol{\Lambda}+\boldsymbol{\gamma}+\boldsymbol{\Delta}) = 0. \tag{22}$$

In this equation

$$\mathbf{Q}^T\boldsymbol{\Delta} = \frac{(\zeta + 2\Omega z)}{a^2}\begin{pmatrix} 0 & -z & y \\ z & 0 & -x \\ -y & x & 0 \end{pmatrix}\begin{pmatrix} X \\ Y \\ Z \end{pmatrix}, \tag{23}$$

and

$$\mathbf{Q}^T\boldsymbol{\Lambda} = \mathbf{P}\nabla_c(gh + \frac{\mathbf{V}\cdot\mathbf{V}}{2}). \tag{24}$$

The vorticity ζ is defined in the spherical coordinate system as $\zeta \equiv \mathbf{k}\cdot\nabla\times\mathbf{v}$. Since the *curl* is invariant under coordinate transformation we have that $\zeta \equiv \mathbf{k}\cdot\nabla_c\times\mathbf{V}$ where $\mathbf{k}$ is the unit vector in the direction normal to the sphere at the point (x, y, z). That is, $\mathbf{k} = \frac{\mathbf{x}}{a}$. (This notation in Cartesian coordinates should not be confused with the standard notation $\mathbf{k}$ for the unit vector in the z-direction.) In terms of Cartesian derivates the *curl* is the standard,

$$\nabla_c \times \mathbf{V} = \begin{pmatrix} \frac{\partial Z}{\partial y} - \frac{\partial Y}{\partial z} \\ \frac{\partial X}{\partial z} - \frac{\partial Z}{\partial x} \\ \frac{\partial Y}{\partial x} - \frac{\partial X}{\partial y} \end{pmatrix}. \tag{25}$$

These derivatives are available from the $\mathbf{C}$ matrix described above.

The rotational form of the momentum equation has one very excellent property for collocation methods[1]. It is semi-energy conserving. This can be seen by considering the discrete kinetic energy equation obtained by multiplication of the momentum equation with the velocity. The troublesome advection term has split into two parts, one horizontal to the surface of the sphere buried in the gradient and the other purely normal to the surface of the sphere. This second term vanishes identically when dotted with a Cartesian velocity that is horizontal to the surface of the sphere.

Using the rotational form gives nonlinear (energy) stability to the numerical method and eliminates the need for artificial diffusion to enhance stability.

3 Local Cartesian Spectral Approximation

The spherical harmonic functions form a basis for functions defined on the surface of the sphere. The spherical harmonic, Y_n^m can be defined in terms of the normalized associated Legendre polynomials $P_n^m(\theta)$ by

$$Y_n^m = \exp^{im\lambda}\bar{P}_n^m. \tag{26}$$

The normalized associated Legendre polynomials can be defined from Rodrigues' formula [10]

$$\bar{P}_n^m(\theta) = (-1)^m\left[\frac{2n+1}{2}\frac{(n-m)!}{(n+m)!}\right]^{1/2}\frac{1}{2^n n!}(\sin\theta)^m\frac{d^{m+n}}{dz^{m+n}}(z^2-1)^n \tag{27}$$

where $z = \cos\theta$ and θ is colatitude. Equations 26 and 27 are combined to give a formula for the Cartesian representation of the spherical harmonics [11].

$$Y_n^m(x,y,z) = C_n^m (x+iy)^m \frac{d^{m+n}}{dz^{m+n}}(z^2-1)^n, \tag{28}$$

where

$$C_n^m = \frac{(-1)^m}{2^n n!}\left[\frac{2n+1}{2}\frac{(n-m)!}{(n+m)!}\right]^{1/2}. \tag{29}$$

Each spatial field can be approximated in Cartesian coordinates by a series of trivariate polynomials. For example,

$$\phi(x,y,z) = \sum_{m,n} c_n^m Y_n^m(x,y,z), \tag{30}$$

where the c_n^m are coefficients of the trivariate polynomials Y_n^m.

To find the c_n^m's in the expression for ϕ, a least squares problem could be solved to fit ϕ data at a set of points on the surface of the sphere with the expansion. Depending on how many points this involves and how many terms are taken in the spectral expansion, this is either a full rank or a rank deficient least squares problem. The singular value decomposition of the system matrix can be used to solve either problem. For the most part we will be concerned with the underconstrained or rank deficient problem. For example, on an icosahedral grid each grid point has 6 or 7 nearest neighbors. Using a second order interpolant, we have 9 degrees of freedom.

4 Discrete Operator Formulas

Rather than interpolating a field and then differentiating the formula we can alternatively approximate the derivative operators or Laplace operator directly by requiring that the discrete operators act correctly on selected basis functions. Given a cluster of points p_l, $l = 0, ..., np-1$ on the surface of the sphere and a tabulation $U(p_l)$ about the point p_0, then we wish to determine coefficients c_l such that

$$L(U)(p_0) \approx \sum_{l=0}^{np-1} c_l U(p_l). \tag{31}$$

The sense of the approximation ($\approx$) will be described shortly. To this end we require 31 to hold for all spherical harmonics through some number N,

$$L(r^n Y_n^m)(p_0) \cong \sum_{l=0}^{np-1} c_l r^n Y_n^m(p_l). \tag{32}$$

This system is then solved for the c_l. A different set of c_l are required for each cluster that is not congruent to another cluster. This procedure is followed for each of the linear operators $L(U) = \frac{\partial U}{\partial x}, \frac{\partial U}{\partial y}, \frac{\partial U}{\partial z}$, and the Laplacian, ΔU. This approach is quite general and is applicable to any distribution of points on the sphere.

The sense of the approximation in (31) is determined by the exact formulation and sense of the approximation in (32). We order the spherical harmonics Y_n^m, so that with increasing number the degree increases, (see the Appendix for a listing of the harmonics as trivariate polynomials). We may require equation (32) to be satisfied with equality for the spherical harmonics through number N_1. In addition, we may require that spherical harmonics up to degree $N_1 + N_2$ satisfy (32) in a least squares sense. The approximation for the derivative so derived will be exact for polynomials of degree less than or equal to the corresponding degree of the N_1 harmonic and will capture some of the higher order behavior.

This formulation leads to a linear least squares problem with equality constraints. The problem can be stated in matrix form: find $\mathbf{c}$ which satisfies

$$\mathbf{H_1 c} = \mathbf{d_1} \tag{33}$$

and minimizes

$$||\mathbf{H_2 c} - \mathbf{d_2}|| \tag{34}$$

where $\mathbf{H_1}$ is a $N_1 \times np$ matrix of the lower order spherical harmonics evaluated at points of the cluster and $\mathbf{H_2}$ is a $N_2 \times np$ matrix of higher order harmonics. The linear least squares problem with equality constraints has a unique solution if and only if

$$rank \begin{pmatrix} \mathbf{H_1} \\ \mathbf{H_2} \end{pmatrix} = np. \tag{35}$$

The least squares problem can be solved elegantly using the singular value decomposition (SVD) [5]. Let $\mathbf{H_1} = \mathbf{USV}^T$ be the SVD with $\mathbf{V} = [\mathbf{K_1}, \mathbf{K_2}]$. With

$$\bar{\mathbf{c}} = \mathbf{VS^{-1}U}^T\mathbf{d_1} \tag{36}$$

the solution to the constrained least squares problem is

$$\mathbf{c} = \bar{\mathbf{c}} + \mathbf{K_2}(\mathbf{H_2K_2})^{\dagger}(\mathbf{d_2} - \mathbf{H_2}\bar{\mathbf{c}}). \tag{37}$$

The computation of the solution thus requires SVD factors be computed for $\mathbf{H1}$ and $\mathbf{H_2K_2}$.

The choice of N_1, N_2 and np determine the formal accuracy and smoothness of the derivative approximations. To obtain consistency of the approximation with the derivative operator, N_1 must be at least 4, i.e. exact for linear functions. The ability to fit higher order harmonics requires that $np > 4$. In general, we choose np points nearly symmetric about the point p_0. The number of points used in the stencil will determine the efficiency of the method because evaluation of the derivatives requires a combination of values from these neighboring points.

q	Grid Points	Triangles	h_{min}(km)	h_{max}(km)	h_{ave}(km)	h_{min}/h_{max}
-	12	20	6699.0	6699.0	6699.0	1.0000
0	42	80	3482.0	3938.0	3710.0	0.8843
1	162	320	1613.0	2070.0	1901.0	0.7792
2	642	1280	761.1	1049.0	956.2	0.7255
3	2562	5120	368.4	526.3	478.8	0.7001
4	10242	20480	181.2	263.4	239.5	0.6878

Figure 1: Geometric information for icosahedral grids

For the icosahedral grid, each point has 5 or 6 immediate neighbors ($np = 7$). If the immediate neighbors of each of these are included in the stencil, then $np = 19$.

One further parameter that can be introduced is the truncation level in the SVD solution. The least squares problem has minimum norm solutions if the number of points is greater than $N2$. For the case $N1 = 0$, we have found it advantageous to use the same truncation at all points. For $np = 7$, we truncate at six because the primary points of the icosahedron have only six modes. So the solution is unique at these points and of minimum norm at the other points. For $np = 19$, the pentagonal points have only 16 immediate neighbors, so we truncate to 16 singular values.

4.1 Numerical Results for the Gradient Approximation

The accuracy of the approximation to the gradient was evaluated with a simple test function on several icosahedral meshes. The basic icosahedral mesh consists of twenty triangles. Each of the twelve points of the mesh is connected to five neighboring points. The refinements of this mesh are accomplished by subdividing each of the twenty base triangles. By placing three points on each side of each large triangle and dividing each triangle into three the $q = 0$ mesh is obtained. Halving this mesh results in the $q = 1$ mesh and again halving gives the $q = 2$ mesh. The number of points in the mesh is given by the formula,

$$N(q) = 5(2^{2q+3}) + 2 \tag{38}$$

Table 1 gives geometric information about the different icosahedral meshes.

In order to check the accuracy of the gradient approximations, a test function which exhibits all modes was used,

$$\phi(\lambda, \theta) = a(\exp x + \exp y + \exp z) \tag{39}$$

The errors in the following tables are derived from the Cartesian approximation to the gradient of this function. The exact values of the function at the vertices of the icosahedral mesh are computed and used in the difference formulas to

Grid points	np	$N1$	error
	$N1 + N2 = 16$		
642	7	0	5.17e-2
642	7	1	3.71e-2
642	7	2	2.67e-2
642	7	3	1.90e-2
642	7	4	7.39e-3
	$N1 + N2 = 16$		
642	19	0	1.77e-4
642	19	1	1.77e-4
642	19	2	1.77e-4
642	19	3	1.77e-4
642	19	4	1.77e-4
	$N1 + N2 = 25$		
642	19	0	2.78e-3
642	19	1	1.92e-3
642	19	2	1.98e-4
642	19	3	1.89e-4
642	19	4	2.32e-5

Figure 2: Gradient Approximation for $q = 2$ with varying $N1$

approximate the Cartesian derivatives. The Cartesian gradient is then transformed to spherical coordinates and compared with the exact gradient of ϕ. The error reported is the l^2-error over the points of the icosahedral mesh.

The first question to be answered regards the choice of $N1$, $N2$ and the number of points in the stencil. Is there an optimal choice for these parameters on a given grid? Table 2 presents the l2 error of the computed versus analytically calculated gradient. The number of constraint equations $N1$ is varied while the sum $N1 + N2$ is held constant. If $N1 + N2 = 9$, then spherical harmonics of second order are used. If $N1 + N2 = 16$, then third order harmonics are included. For $N1 + N2 = 25$, fourth order harmonics are included.

Plotting the results, in Figure 3, for the case $N1 = 0$ with a log-log scale shows the first, second or third order convergence of the approximation as the mesh size is decreased.

5 Test Cases

A set of test cases for the shallow water equations on a sphere are detailed in [18]. These cases are provide a rigorous test of methods as well as allowing for comparison between methods. Several of these are documented for the Cartesian method.

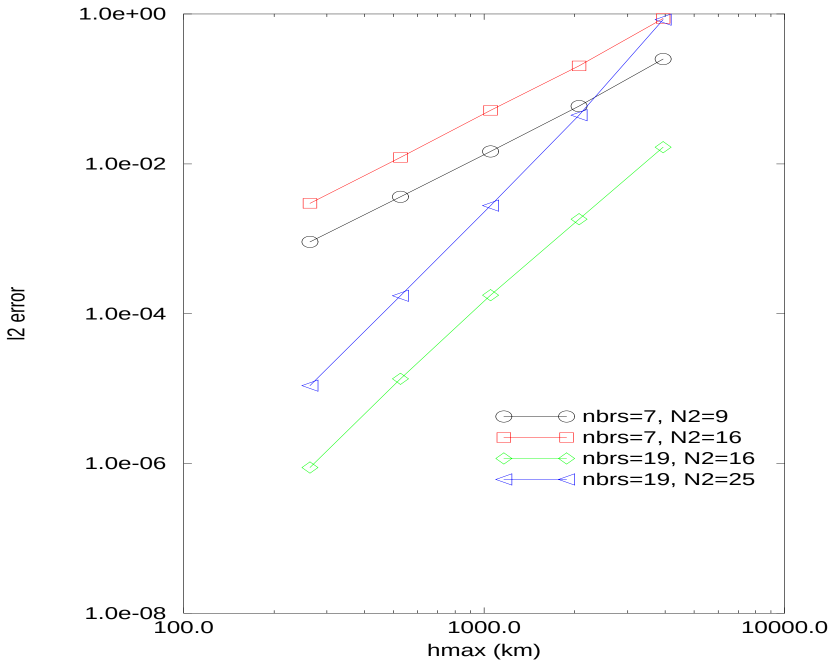

Figure 3: Convergence of the Gradient Approximations, $N1 = 0$.

5.1 Advection Test

Test case 1 is a pure advection problem in which a cosine bell is blown around the sphere under a constant velocity field. Figure 4 shows the relative RMS error in the geopotential field as a function of time for a variety of grids. The operators are approximated with quadratic spherical harmonics and use only nearest neighbors. No diffusion was used for this case.

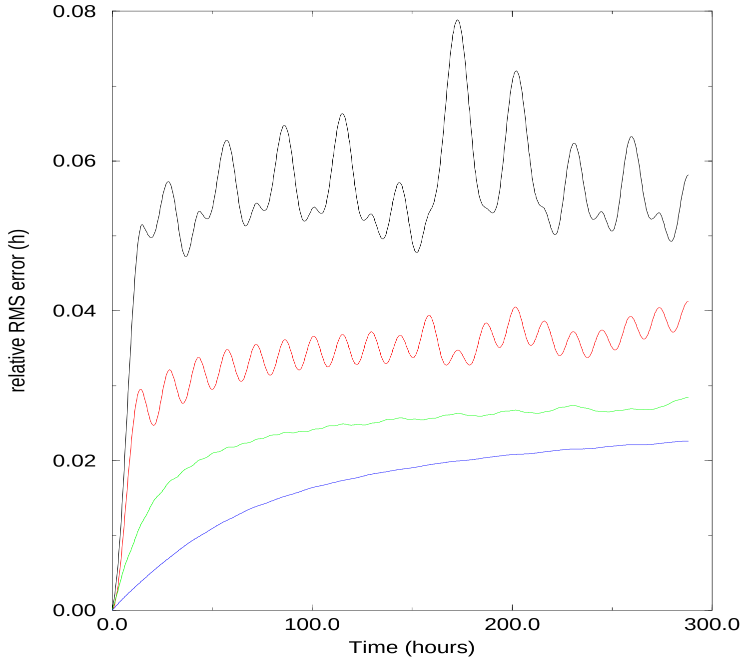

Figure 4: Relative RMS Error in height, Test Case 1, $q = 1, 2, 3, 4$.

The second order approximation obtained by using 9 harmonics on 16-19 points does not require the addition of artificial diffusion to maintain stability. This is because of the smoothing property of an interpolant which fits more points than functions. Table 5 shows the relative l_{inf} and relative l_{inf} error for different meshs at the end of the 12 day simulation.

5.2 Steady, Zonal Flow Test

Test case 2 is a steady, non-linear zonal flow rotated through an angle $\alpha = \frac{\pi}{4}$. It tests the ability of the code to maintain a steady state solution independent of the grid orientation and gives a good idea of the accuracy of the methods. The velocity and geopotential for this test case are exactly representable with the spherical harmonics of second order. So the local spherical harmonic ap-

Grid q	$l_{\inf}$	l_2
2	6.832E-01	1.188E+00
3	3.557E-01	5.180E-01
4	6.419E-02	8.480E-02

Figure 5: Final Error in Case 1 for $q = 2, 3, 4$. N1=0, N2=9, npts=19

proximations for the derivative operators are able to capture the steady state solution extremely well. Figure 6 and 7 show the error, as a function of time, in the velocity (using the relative RMS error with the exact steady solution) and the RMS error in the height field, respectively. Since the model includes no damping the error builds after a time and then grows exponentially. The $q = 2, 3$integrations used a time step of 1200 seconds for the 5 day (120 hour) simulations while the $q = 4$ mesh used a 600 second timestep. The momentum equation was modified with a diffusion operator $\epsilon_V \Delta V$ where $\epsilon_V = 8000$. Similarly the height equation was modified with a diffusion coefficient of $\epsilon_h = 20000$.

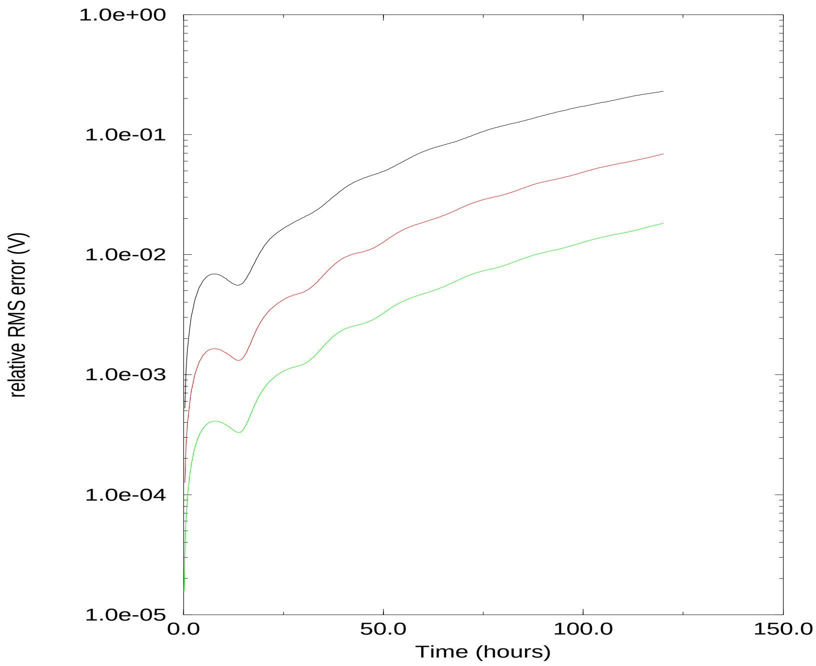

Figure 6: Relative RMS Error in velocity, Test Case 2, $q = 2, 3, 4$. Standard Form

The rotational form gives somewhat better results with no diffusion added. Figure 8 and 9 show the velocity error and the height error for the rotational form

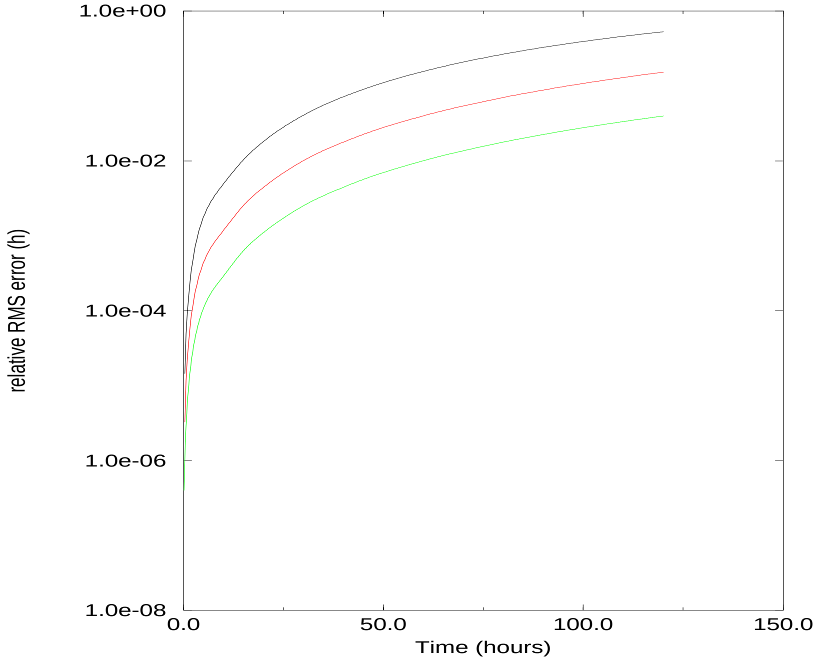

Figure 7: Relative RMS Error in height, Test Case 2, $q = 2, 3, 4$. Standard Form

of the Cartesian equations also using the serendipitous quadratic approximation on 6 or 7 neighbors. The error growth is much more controlled.

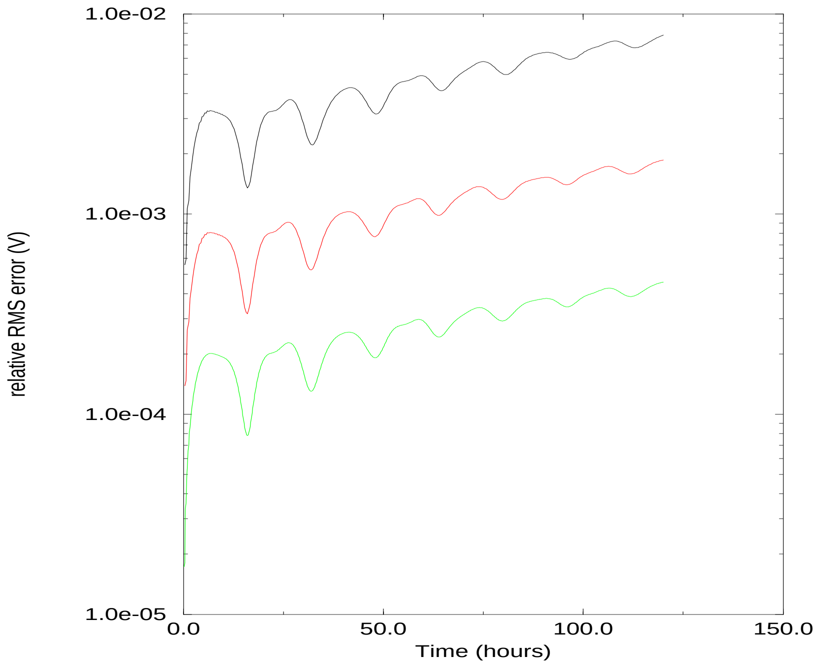

Figure 8: Relative RMS Error in Velocity, Test Case 2, $q = 2, 3, 4$. Rotational Form

A contor plot of the absolute geopotential error is given in figure 10. The error is measured at the 5 days. Clearly evident are the base points of the icosahedral grid where the difference stencil involves 6 rather than 7 points.

5.3 Non-Analytic, Steady, Zonal Flow Test

Test case 3 is a steady, non-linear zonal flow rotated through some angle $\alpha = \frac{\pi}{3}$. It is similar to test case 2 but has profiles which are not exactly representable by the spherical harmonics since they are of compact support. The local spherical harmonic approximations for the derivative operators are able to capture the steady state solution but not as well as in Test case 2. Figure 11 and 12 show the error, as a function of time, in the velocity (using the relative RMS error with the exact steady solution) and the RMS error in the height field, respectively. Since the model includes no damping the error builds after a time and then grows exponentially. The $q = 2, 3$integrations used a time step of 1200 seconds for the 5 day (120 hour) simulations while the $q = 4$ mesh used a 600 second timestep. For this case, no explicit diffusion was added to either the momentum

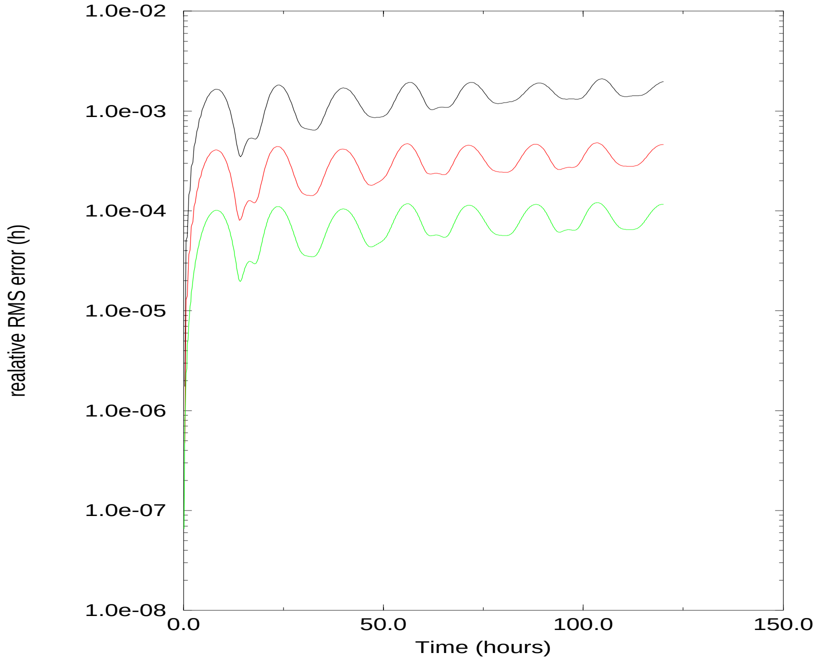

Figure 9: Relative RMS Error in Height, Test Case 2, $q = 2, 3, 4$. Rotational Form

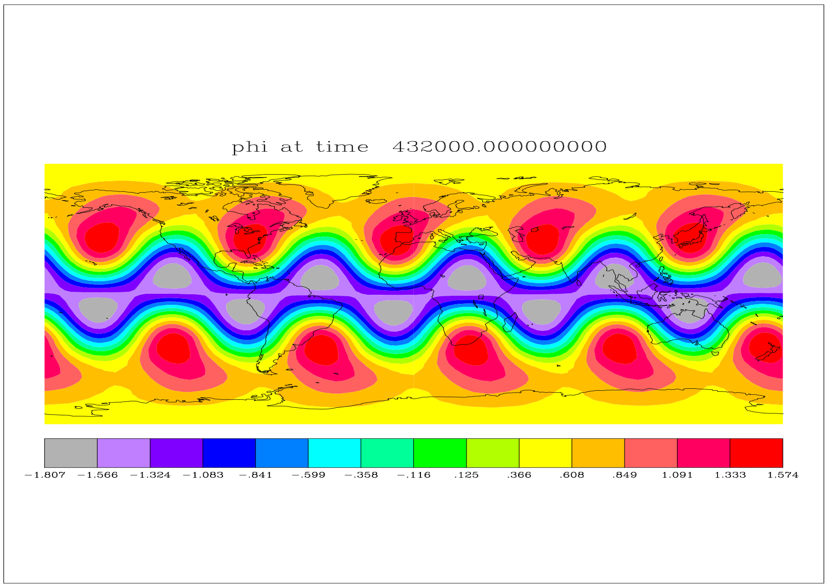

Figure 10: Error in Geopotential at 5 days, Test Case 2, $q = 4$. Rotational Form

or height equations.

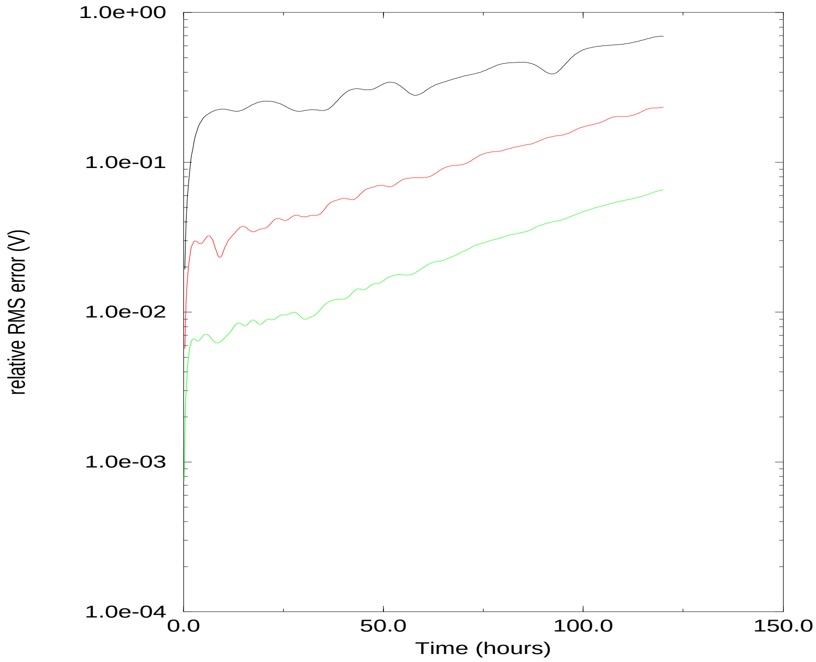

Figure 11: Relative RMS Error in Velocity, Test Case 3, $q = 2, 3, 4$. Standard Form

The rotational form error results for case 3 are given in figures 13 and 14.

A contor plot of the absolute geopotential error is given in figure 15. The error is measured at the 5 days.

The second order method on 16-19 points without diffusion gives errors as follows A growth in the error on the fine mesh seems to indicate a lack of energy conservation and the associated growth in error. Adding a modest amount of diffusion with $\epsilon = 8.e3$, gives similar results.

5.4 Zonal Flow Over an Isolated Mountain

This test case is the only one with orography. A 5400m mountain is given through the surface height function, h_s. No analytical solution is known for this case so the usefulness of the case is in diagnosing the conservation properties of the numerical scheme. The following normalized integral quantities are presented as a function of time: mass, total energy, potential enstrophy. The vorticity is presented as an integral without normalization in figure 17.

A contor plot of the geopotential at 15 simulated days is given in figure 18.

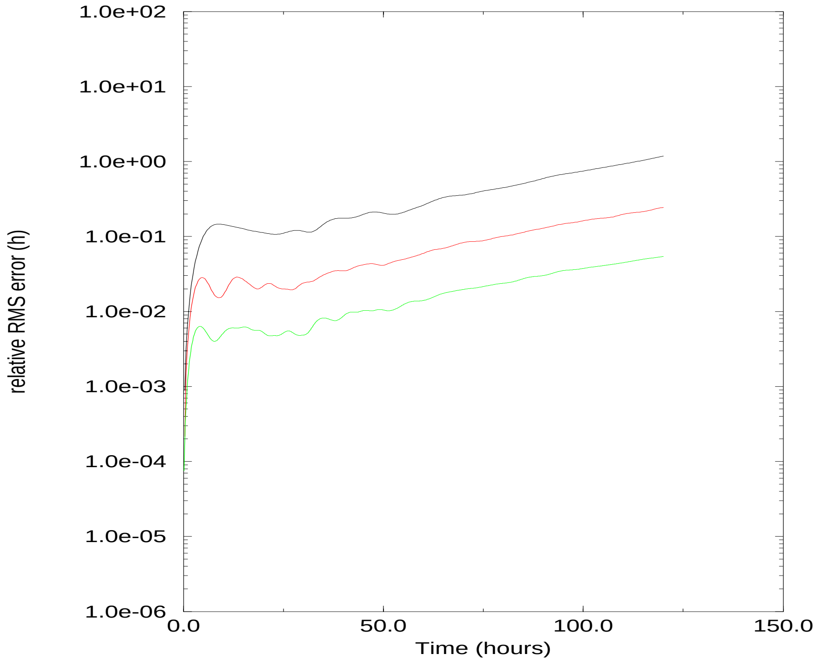

Figure 12: Relative RMS Error in Height, Test Case 3, $q = 2, 3, 4$. Standard Form

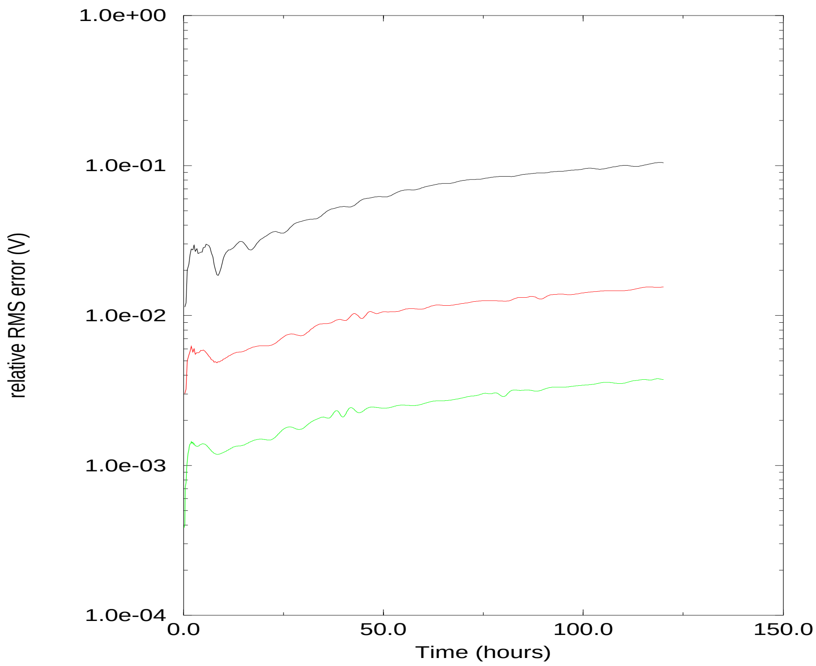

Figure 13: Relative RMS Error in Velocity, Test Case 3, $q = 2, 3, 4$. Rotational Form

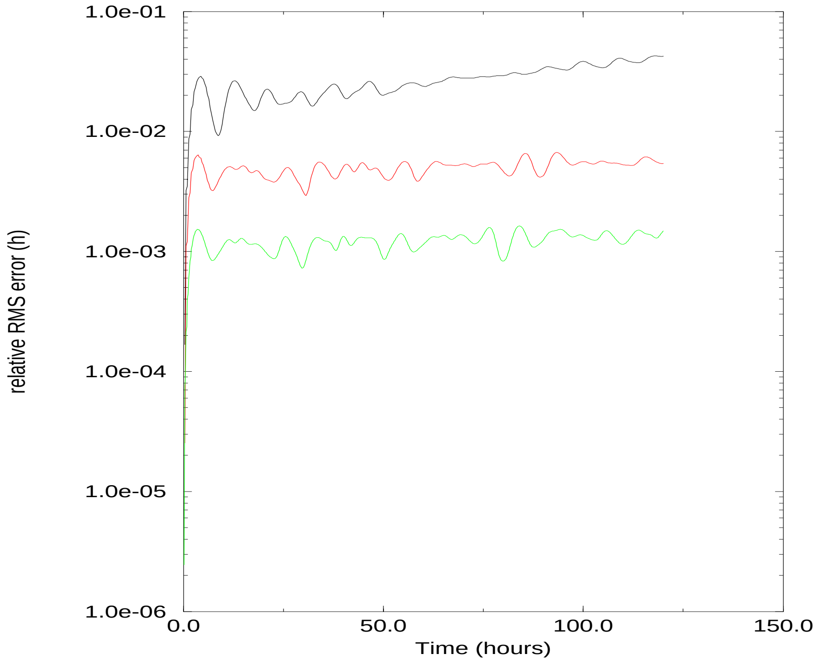

Figure 14: Relative RMS Error in Height, Test Case 3, $q = 2, 3, 4$. Rotational Form

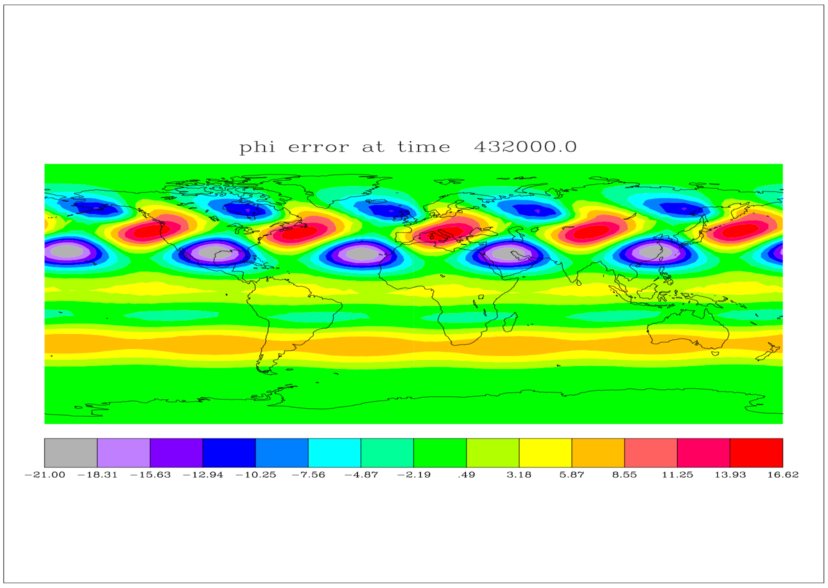

Figure 15: Error in Geopotential at 5 days, Test Case 3, $q = 4$. Rotational Form

Grid q	$l_{\text{inf}}(\phi)$	$l_2(\phi)$	$l_{\text{inf}}(V)$	$l_2(V)$
2	4.291E-01	3.265E-01	6.260E-01	6.107E-01
3	5.006E-02	2.256E-02	1.192E-01	8.043E-02
4	7.491E-01	2.828E-01	1.013E+00	4.694E-01

Figure 16: Final Error in Case 3 for $q = 2, 3, 4$. N1=0, N2=9, npts=19

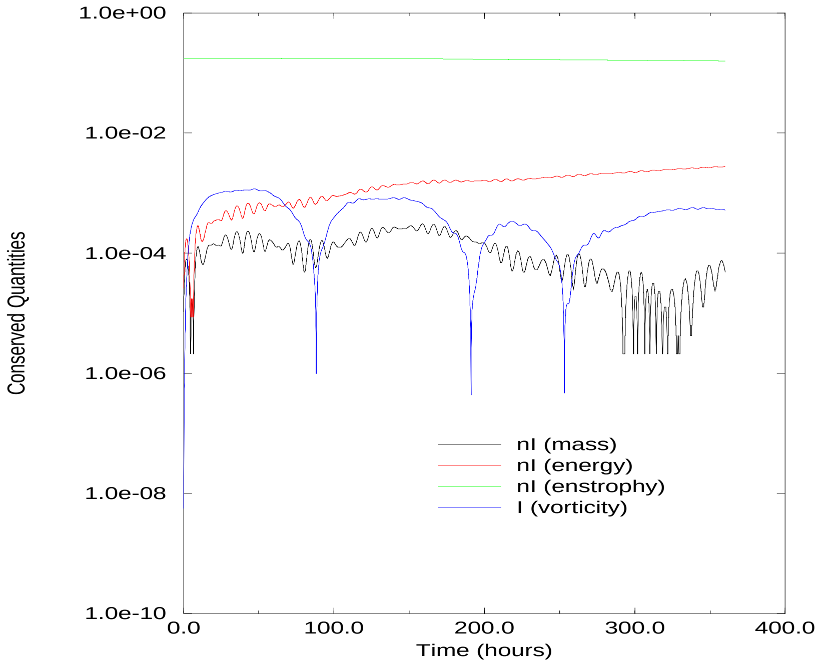

Figure 17: Conserved integral quantities. Test Case 5, $q = 4$. Rotational Form

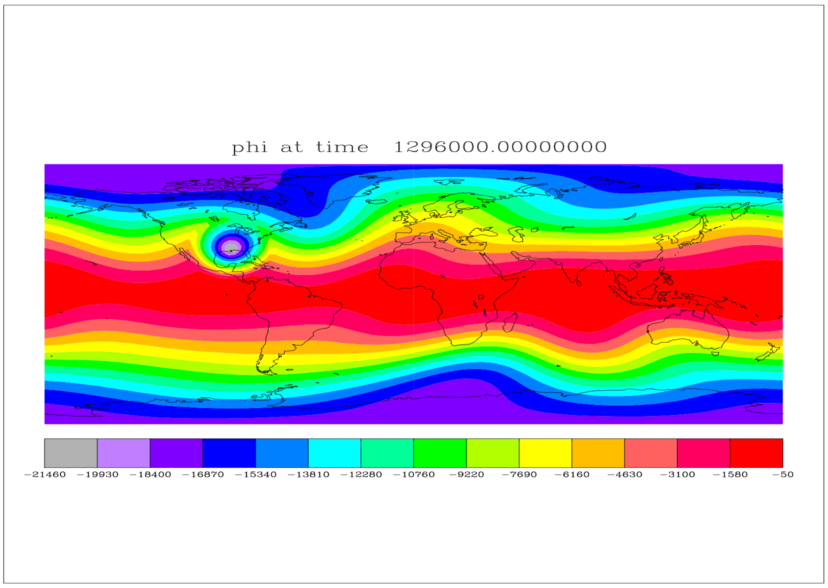

Figure 18: Geopotential at 15 days, Test Case 5, $q = 4$. Rotational Form

5.5 Rossby-Haurwitz Wave

This classic standard test case [7] does not have an analytic solution for the nonlinear shallow water equations. The initial conditions are zonal wave number 4. The solution at 0, 7, and 14 days continues to show the strong influence of the initial conditions. A diffusion coefficient of $\epsilon_V = 5 \times 10^5$ was used for these calculations. Interestingly, this is close to the value of the diffusion coefficient used by Richardson in [8] and also by Williamson in [15]. However, unlike the latter study, we find that the diffusion required for stability on finer grids decreases rather than increases.

The rotational form is semi-conservative of energy. Figures 19 shows the conserved quantities of mass, energy, enstrophy as normalized integrals and the conserved integral of vorticity through the simulation.

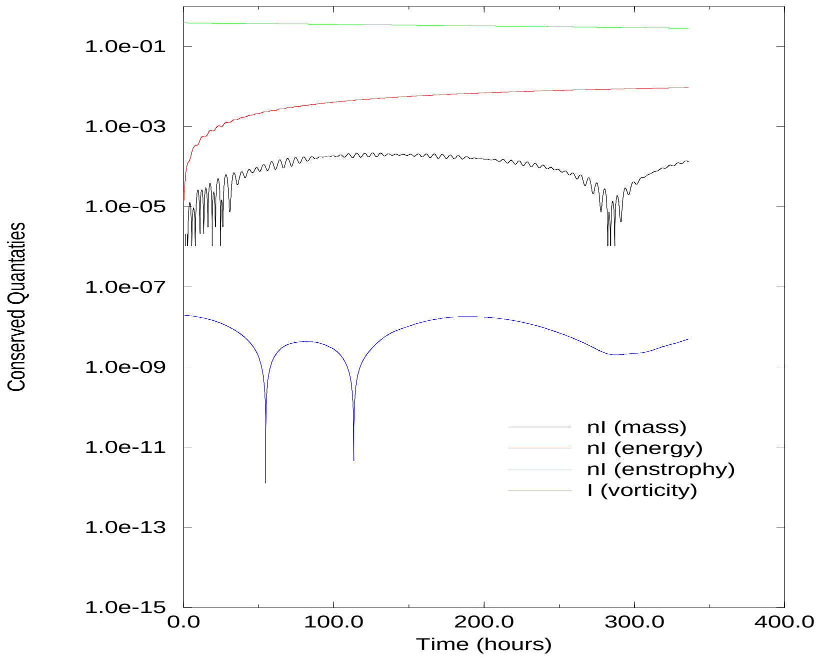

Figure 19: Conserved integral quantities. Test Case 6, $q = 4$. Rotational Form

A contor plot of the geopotential at 14 simulated days is given in figure 20.

5.6 Conclusions

Numerical methods for the shallow water equations on the sphere, or generally any PDE on the sphere, are faced with three hurdles. First, the accuracy of the geostrophic wind balance. The numerical approximation for the gradient of

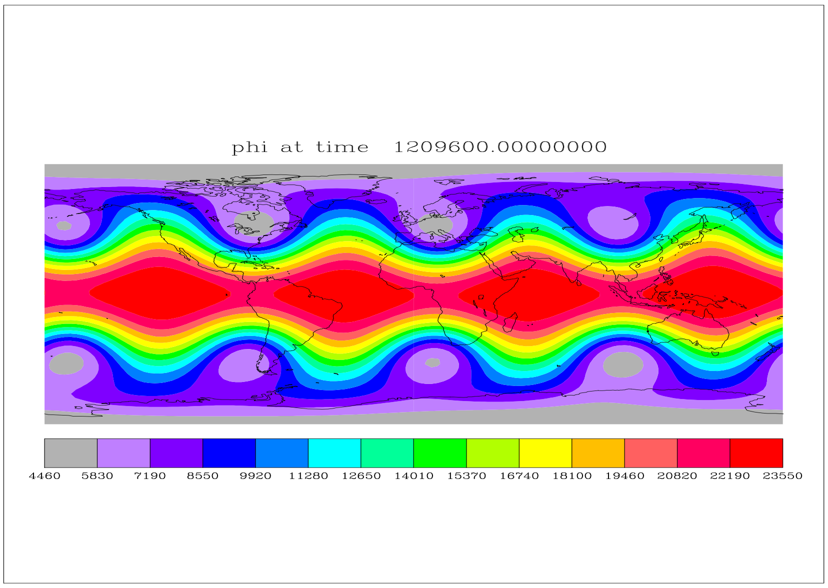

Figure 20: Geopotential at 14 days, Test Case 6, $q = 4$. Rotational Form

the geopotential must balance the Coriolis term well. Since the Coriolis term does not involve derivatives the gradient approximation is crucial to achieve a reasonable balance. Second, the pole problem. Since the spherical coordinate representation of the velocity is singular at the poles and derivatives are approximated only with care, this can prove to be a formidable problem. The third hurdle is stability. As nonlinear equations, the energy consistency of conversion terms from potential to kinetic energy play a crucial role. In our work, the first hurdle has been passed by adopting a co-located velocity and gradient approximation. The collocation method with accurate approximations for the derivatives gives an excellent balance of the geostrophic wind terms. The Cartesian method is free of the pole problem since velocities are continuous at the poles. Finally, the rotational form of the equations in Cartesian form gives the required energy conservation to maintain stability.

The serendipitous use of least squares fitting of the quadratic spherical harmonics to a seven point stencil has given second order convergence for the price of something less.

References

[1] C. Canuto, M.Y. Hussaini, A. Quarteroni, and T.A. Zang. *Spectral Methods in Fluid Dynamcis*. Springer-Verlag, Berlin, 1988.

[2] I-Liang Chern. A control volume method on a icosahedral grid for numerical integration of the shallow-water equations on the sphere - i. Mcs preprint, Argonne National Laboratory, Chicago, IL, 1991.

[3] Ross Heikes and David A. Randall. Numerical integration of the shallow-water equations on a twisted icosahedral grid. part i. *Mon. Wea. Rev.*, 123:1862–1880, 1995.

[4] Ross Heikes and David A. Randall. Numerical integration of the shallow-water equations on a twisted icosahedral grid. part ii. *Mon. Wea. Rev.*, 123:1881–1887, 1995.

[5] C.L. Lawson and R.J. Hanson. *Solving Least Squares Problems*. Prentice-Hall, Englewood Cliffs, NJ, 1974.

[6] Y. Masuda and H. Ohnishi. An integration scheme of the primitive equation model with an icosahedral-hexagonal grid system and its application to the shallow water equations. In *Short- and Medium-Range Numerical Weather Prediction*, pages 317–326, 1986.

[7] N. A. Phillips. Numerical integration of the primitive equations on the hemisphere. *Mon. Wea. Rev.*, 87:333–345, 1959.

[8] L.F. Richardson. Atmospheric diffusion shown on a distance neighbour graph. *Proc. Roy. Soc. Ser. A*, 110:709–737, 1928.

[9] R. Sadourny, A. Arakawa, and Y. Mintz. Integration of the nondivergent barotropic vorticity equation with an icosahedral-hexagonal grid for the sphere. *Mon. Wea. Rev.*, 96:351–356, 1968.

[10] I. A. Stegun. Legendre functions. In M. Abramowitz and I. A. Stegun, editors, *Handbook of Mathematical Functions*, chapter 8, pages 332–353. Dover Publications, New York, 1972.

[11] A.N. Tikhonov and A.A. Samarskii. *Equations of Mathematical Physics*. Dover Publications, New York, 1963.

[12] D. L. Williamson. Integration of the barotropic vorticity equation on a spherical geodesic grid. *Tellus*, 20:642–653, 1968.

[13] D. L. Williamson. Integration of the primitive barotropic model over a spherical geodesic grid. *Mon. Wea. Rev.*, 98:512–520, 1969.

[14] D. L. Williamson. Numerical integration of fluid flow over triangular grids. *Mon. Wea. Rev.*, 97:885–895, 1969.

[15] D. L. Williamson. A comparison of first- and second-order difference approximations over a spherical geodesic grid. 7, 1971.

[16] D. L. Williamson. *Numerical Methods Used in Atmospheric Models*, chapter 2, pages 51–120. GARP Pub. Ser. No. 17. JOC, WMO, Geneva, Switzerland, 1979.

[17] D. L. Williamson and G. L. Browning. Comparison of grids and difference approximations for numerical weather prediction over a sphere. *J. Appl. Meteor.*, 12:264–274, 1973.

[18] D. L. Williamson, J.B. Drake, J.J. Hack, Rudiger Jakob, and P.N. Swarztrauber. A standard test set for numerical approximations to the shallow water equations on the sphere. *J. Comp. Phys.*, pages 211–224, 1992.

6 Appendix: Spherical Harmonic Polynomials

$n = 0$:

$$Y_0^0 = 1$$

$n = 1$:

$$\begin{aligned} rY_1^0 &= z \\ rY_1^1 &= -x - \mathbf{i}\, y \end{aligned}$$

$n = 2$:

$$\begin{aligned} r^2Y_2^0 &= \frac{3}{2} z^2 - \frac{1}{2} \\ r^2Y_2^1 &= -3\,(x + \mathbf{i}\, y)\, z \\ r^2Y_2^2 &= 3\,x^2 + 6\,\mathbf{i}\, x\, y - 3\,y^2 \end{aligned}$$

$n = 3$:

$$\begin{aligned} r^3Y_3^0 &= z^3 + \frac{3}{2}(z^2 - 1)\, z \\ r^3Y_3^1 &= -\frac{1}{48}(x + \mathbf{i}\, y)(360\, z^2 - 72) \\ r^3Y_3^2 &= 15\,(x^2 + 2\,\mathbf{i}\, x\, y - y^2)\, z \\ r^3Y_3^3 &= -15\, x^3 + 45\, x\, y^2 - 15\,\mathbf{i}\,(3\, x^2\, y - y^3) \end{aligned}$$

$n = 4$:

$$\begin{aligned}
r^4 Y_4^0 &= z^4 + 3\,(\,z^2 - 1\,)\,z^2 + \frac{3}{8}\,(\,z^2 - 1\,)^2 \\
r^4 Y_4^1 &= -\frac{1}{384}\,(\,x + \mathbf{i}\,y\,)\,(\,3840\,z^3 + 2880\,(\,z^2 - 1\,)\,z\,) \\
r^4 Y_4^2 &= \frac{1}{384}\,(\,x^2 + 2\,\mathbf{i}\,x\,y - y^2\,)\,(\,20160\,z^2 - 2880\,) \\
r^4 Y_4^3 &= -105\,(\,x^3 - 3\,x\,y^2 + \mathbf{i}\,(\,3\,x^2\,y - y^3\,)\,)\,z \\
r^4 Y_4^4 &= 105\,x^4 - 630\,x^2\,y^2 + 105\,y^4 + 105\,\mathbf{i}\,(\,4\,x^3\,y - 4\,x\,y^3\,)
\end{aligned}$$

$n = 5$:

$$\begin{aligned}
r^5 Y_5^0 &= z^5 + 5\,(\,z^2 - 1\,)\,z^3 + \frac{15}{8}\,(\,z^2 - 1\,)^2\,z \\
r^5 Y_5^1 &= -\frac{1}{3840}\,(\,x + \mathbf{i}\,y\,)\,\left(57600\,z^4 + 86400\,(\,z^2 - 1\,)\,z^2 + 7200\,(\,z^2 - 1\,)^2\right) \\
r^5 Y_5^2 &= \frac{1}{3840}\,(\,x^2 + 2\,\mathbf{i}\,x\,y - y^2\,)\,(\,403200\,z^3 + 201600\,(\,z^2 - 1\,)\,z\,) \\
r^5 Y_5^3 &= -\frac{1}{3840}\,(\,x^3 - 3\,x\,y^2 + \mathbf{i}\,(\,3\,x^2\,y - y^3\,)\,)\,(\,1814400\,z^2 - 201600\,) \\
r^5 Y_5^4 &= 945\,(\,x^4 - 6\,x^2\,y^2 + y^4 + I\,(\,4\,x^3\,y - 4\,x\,y^3\,)\,)\,z \\
r^5 Y_5^5 &= -945\,x^5 + 9450\,x^3\,y^2 - 4725\,x\,y^4 - 945\,\mathbf{i}\,(\,5\,x^4\,y - 10\,x^2\,y^3 + y^5\,)
\end{aligned}$$

$n = 6$:

$$\begin{aligned}
r^6 Y_6^0 &= z^6 + \frac{15}{2}\,(\,z^2 - 1\,)\,z^4 + \frac{45}{8}\,(\,z^2 - 1\,)^2\,z^2 + \frac{5}{16}\,(\,z^2 - 1\,)^3 \\
r^6 Y_6^1 &= -\frac{1}{46080}(\,x + \mathbf{i}\,y\,)\,\left(967680\,z^5 + 2419200\,(\,z^2 - 1\,)\,z^3 + 604800\,(\,z^2 - 1\,)^2\,z\right) \\
r^6 Y_6^2 &= \frac{1}{46080}(\,x^2 + 2\,\mathbf{i}\,x\,y - y^2\,) \\
&\quad \left(9676800\,z^4 + 9676800\,(\,z^2 - 1\,)\,z^2 + 604800\,(\,z^2 - 1\,)^2\right) \\
r^6 Y_6^3 &= -\frac{1}{46080} \\
&\quad (\,x^3 - 3\,x\,y^2 + \mathbf{i}\,(\,3\,x^2\,y - y^3\,)\,)\,(\,58060800\,z^3 + 21772800\,(\,z^2 - 1\,)\,z\,) \\
r^6 Y_6^4 &= \frac{1}{46080} \\
&\quad (\,x^4 - 6\,x^2\,y^2 + y^4 + \mathbf{i}\,(\,4\,x^3\,y - 4\,x\,y^3\,)\,)\,(\,239500800\,z^2 - 21772800\,) \\
r^6 Y_6^5 &= -10395\,(\,x^5 - 10\,x^3\,y^2 + 5\,x\,y^4 + \mathbf{i}\,(\,5\,x^4\,y - 10\,x^2\,y^3 + y^5\,)\,)\,z \\
r^6 Y_6^6 &= 10395\,x^6 - 155925\,x^4\,y^2 + 155925\,x^2\,y^4 - 10395\,y^6
\end{aligned}$$

$$+\,10395\,\mathbf{i}\,(\,6\,x^5\,y-20\,x^3\,y^3+6\,x\,y^5\,)$$